Fermi National Accelerator Laboratory

FERMILAB-Pub-79/37-EXP
7160.095

(Submitted to Phys. Rev. Lett.)

INCLUSIVE π^0 PRODUCTION OVER LARGE $X_\perp$ AND X_F RANGES IN 200, 300, AND 400 GeV/c PROTON-BERYLLIUM INTERACTIONS

R. M. Baltrusaitis, M. Binkley, B. Cox,
T. Kondo, C. T. Murphy, and W. Yang
Fermi National Accelerator Laboratory, Batavia, Illinois 60510

and

L. Ettlinger, M. S. Goodman, J. A. J. Matthews, and J. Nagy
Department of Physics, The Johns Hopkins University, Baltimore, Maryland 21218

June 1979

INCLUSIVE π^o PRODUCTION OVER LARGE $X_\perp$ AND X_F RANGES IN 200, 300, AND 400 GeV/c PROTON-BERYLLIUM INTERACTIONS

R. M. Baltrusaitis, M. Binkley, B. Cox
T. Kondo, C. T. Murphy, and W. Yang
Fermi National Accelerator Laboratory
Batavia, Illinois 60510

and

L. Ettlinger,[a] M. S. Goodman,[b]
J. A. J. Matthews, and J. Nagy[c]
Department of Physics, The Johns Hopkins University
Baltimore, Maryland 21218

Measurements of recognized π^o production in pBe collisions for $.1 < X_\perp < .5$ and $-.8 < X_F < .0$ at 200, 300, and 400 GeV/c are presented. These invariant cross sections are fit by $E\frac{d\sigma}{dp^3} = A(1-X_R)^M P_\perp^{-N}$ over this range of $X_\perp$ and X_F with $M = 4.88 \pm .14$ and $N = 8.90 \pm .10$ independent of energy. No significant evidence for breaking of this scaling is observed over this large kinematic region at these energies.

The measurement of high $P_\perp$ and large X_F inclusive production of π^o's in pN collisions has been the object of a number of experiments at Fermilab[1-8] and the CERN ISR.[9-17] These experiments have attempted to determine whether the invariant cross section can be described over the entire kinematic range and at all energies by a factorized scaling form[18-21] in $P_\perp$ and the radial scaling variable $X_R = \sqrt{X_F^2+X_\perp^2}$

$$E\frac{d\sigma}{dp^3}=F(P_\perp)G(X_R) \qquad (1)$$

We report the results of a measurement of $E\frac{d\sigma}{dp^3}$ over a large range of $P_\perp$ and X_R at 200, 300, and 400 GeV/c in the halo free proton beam[22] of the west branch of Proton Area at Fermilab. We have compared these cross sections to the explicit form

$$E\frac{d\sigma}{dp^3}=A\cdot(P_\perp)^{-N}\ (1-X_R)^M \qquad (2)$$

The experimental apparatus shown in Fig. 1 consisted of a two-arm photon spectrometer. Each arm contained collimators, a 10kG-meter sweeping magnet, a 6 plane MWPC system and a 25 element lead glass Čerenkov counter array along with lucite (L1, L2, L3) and scintillation (S1, S2) counters which were used to impose the trigger requirement of a neutral particle entering the array. The two spectrometer arms were not identical. The lead glass arrays were 260" and 240" from the thin transmission targets, having 2.0 and 2.6 millisteradians of acceptance respectively. The two photons from π^o's were both detected in one or the other of the two arms of the spectrometer which were triggered independently. Data were taken at 200, 300, and 400 GeV with the arm angles varied from 5.8^o to 18.5^o in the

laboratory system (90^{o}-150^{o}cms). For the data reported in this paper, thin foil beryllium targets (8 and 34 mil) were used and the cross sections per nucleon are quoted assuming a linear A dependence. Measurements of the atomic weight dependence of the inclusive cross section, which have been made in this experiment,[23] indicate that this assumption does not affect the results appreciably.

The trigger for the π^{o} events consisted of the requirement that no charged particle be seen in the lucite hodoscope (L1 and L2 off) and that a minimum energy be observed in the lead glass array of either arm. High and low threshold runs were made at each beam energy and angular setting. The cross sections independently determined from each arm agree within assigned errors.

The position of each of the photons from the π^{o} decay was determined by fitting the observed fractional energy deposit in each 2-1/2" by 2-1/2" by 24 radiation length element of the lead glass array to the predictions obtained from shower calculations.[24] These calculations were checked by measurements of the actual transverse shower development produced by 4 to 32 GeV/c electrons from an electron beam[25] which was constructed from elements of the P-West proton transport in order to allow calibration in situ of the detector. Suitable minor modifications of the predicted sharing patterns were introduced in order to match these data. This technique is described elsewhere.[26] The achievable position resolution for the array was approximately $\sigma \sim 0.25$".

The linearity of the lead glass array was measured to be better than 0.5% up to 30 GeV using the calibration beam. Each of the elements of the array was calibrated before and after each run with this same beam. The gains of each phototube were tracked between these calibrations using a set of hydrogen thyratron light sources monitored against a standard ^{241}Am source. By these techniques the mass of π^o peak could be kept stable to ±1% during the few week periods between electron beam calibrations. The fundamental resolution of the lead glass counters was measured[27] to be $7.5\%/\sqrt{E}$ (standard deviation) in a calibration run in a $\frac{\Delta p}{p} = \pm 1\%$ electron beam in the C station at SLAC.

The incident proton flux, which varied from 10^{10} to 10^{12} protons per 1 second spill during the course of the running, was measured by two secondary emission monitors. The systematic error in the absolute measurement of flux arises mainly from the errors in the foil activation cross sections needed to calibrate these devices and is estimated to be less than 5%. The beam loading of the lead glass counters was measured by comparing on every beam pulse the hydrogen thyratron pulser peaks during spill and between spills. Shifts of gains due to loading of the transistorized bases was observed to average less than 1% over the arrays. The dead time was constantly monitored for each data set and was of order 20% for the inclusive π^o measurement. The probability that a π^o event was vetoed by the presence of charged particles was monitored by measuring the fluxes of charged particles in the

non-triggered arm. The correction to the cross section is typically 10% for this data. Finally the loss of data due to conversions of one or both of the two π^o photons has been corrected by measuring the conversion probability in the front two layers of the lucite hodoscope for photons from π^o's for data samples which require only a total energy trigger. This probability was measured to be 16±2% for a single photon independent of photon energy.

Examples of the two photon mass spectrum at different angles and trigger energy thresholds are shown in Fig. 2a and 2b. The two-photon background shapes were calculated assuming that the two photons were from uncorrelated π^o's, with the observed inclusive $P_\perp$ and X_F distributions. The fitted backgrounds under the π^o, which depended mainly on threshold energy and were independent of arm angle, ranged from 20% at low thresholds to 5% for data sets with higher thresholds.

In Fig. 3a, b, and c and Table I the invariant cross sections $E\frac{d\sigma}{dp^3}$ are displayed as a function of $P_\perp$ for bands of X_F for the three beam energies used in this experiment. The relatively gentle variation of $E\frac{d\sigma}{dp^3}$ with X_F can be seen at all three beam energies. A two dimensional fit has been made to the cross section as function of X_R and $P_\perp$ to the form Eq.(2). The results are given in Table II. If data is distributed in X_R and $P_\perp$ according to Eq.(2) then the product $(P_\perp)^N \cdot E\frac{d\sigma}{dp^3}$ should be a function only of X_R and therefore be independent of center of mass angle of the π^o (θ_{cms}) at fixed X_R. In Fig. 4 the

product $P_\perp^{9.0} \cdot E\frac{d\sigma}{dp^3}$ is displayed as a function of θ_{cms} for different X_R bands for the 200 GeV/c data. The distributions are clearly flat, demonstrating the θ_{cms} independence of the data.

Furthermore, if Eq.(2) essentially describes the cross section for π^o production, then $(1-X_R)^{-M} \cdot E\frac{d\sigma}{dp^3}$ vs. $P_\perp$ will explicitly display the $P_\perp$ dependence of the data. In Fig. 5a this product (with M set equal to 5 as indicated by the two dimensional fits) is plotted vs. $P_\perp$ for the three beam energies used in the experiment. The $P_\perp^{-9}$ behavior can clearly be seen at all energies. The fits to the data at each energy are shown separately. In addition, the obvious equality of all cross sections at all three energies at a given $P_\perp$ demonstrates that scaling is good over this energy range. Over the large $X_\perp$ range probed in this experiment no flattening of the $P_\perp$ distribution such as that reported at the ISR[11,17] have been observed.

Finally, the complementary plot to Fig. 5a is the plot of $P_\perp^9 \cdot E\frac{d\sigma}{dp^3}$ vs. X_R. The variation of this product with X_R is shown for the three beam energies in Fig. 5b. As is shown in Fig. 5b and recorded in Table II, $(1-X_R)^{4.9}$ is the preferred fit for all energies but the data may be somewhat steeper at 400 GeV/c for the few low statistics, high X_R points. However, the data are clearly inconsistent with $(1-X_R)^9$ at all energies and scaling is clearly good in the high statistics region.

We would like to express our thanks to the personnel of the Proton Department at Fermilab. We wish to acknowledge the many contributions of Leon Madansky to this experiment. In addition, we acknowledge the help of many other people during the course of this experiment including the early support and efforts of T. Toohig, J. Spangler, A. Pevsner, C. Y. Chien, and B. Barnett. Finally we wish to thank J. Dally, D. Wilson, K. Thomas, and R. Miksa for their help in constructing and running the experiment. This work was supported in part by the U. S. Department of Energy, the Research Corporation of America and the National Science Foundation.

REFERENCES

[a]Present address: Mitre Corporation, Metrek Division, McLean, Virginia

[b]Present address: Harvard University, Physics Department Cambridge, Massachusetts

[c]Present address: Brookhaven National Laboratory Upton, Long Island, New York 11973

[1]J. W. Cronin et al., Phys. Rev. D11, 3105 (1975).

[2]G. Donaldson et al., Phys. Rev. Lett. 36, 1110 (1976).

[3]G. Donaldson et al., Phys. Rev. Lett. 40, 917 (1978).

[4]G. Donaldson et al., Phys. Rev. Lett. 73B, 375 (1978).

[5]D. Antreasyan et al., Phys. Rev. Lett. 38, 105 (1977).

[6]D. C. Carey et al., Phys. Rev. Lett. 33, 327 (1974).

[7]D. C. Carey et al., Phys. Rev. Lett. 33, 330 (1974).

[8]F. E. Taylor et al., Phys. Rev. D. 14, 1217 (1976).

[9]F. W. Büsser et al., Phys. Lett. 46B, 471 (1973).

[10]F. W. Büsser et al., Nucl. Phys. B106, 1 (1976).

[11]A. L. S. Angelis et al., Phys. Lett. 79B, 505 (1978).

[12]K. Eggert et al., Nucl. Phys. B98, 49 (1975).

[13]K. Eggert et al., Nucl. Phys. B98, 73 (1975).

[14]A. G. Clark et al., Nucl. Phys. B142, 180 (1978).

[15]A. G. Clark et al., Phys. Lett. 74B, 267 (1978).

[16]C. Kourkoumelis et al., CERN EP 79-12, 14 Feb., 79.

[17]C. Kourkoumelis et al., CERN EP 79-29, 10 April, 79.

[18]R. P. Feynman, Phys. Rev. Lett. 23, 2159 (1969).

[19]K. Kinoshita and H. Noda, Prog. Theor. Phys., 46, 1639 (1971).

[20]K. Kinoshita and H. Noda, Prog. Theor. Phys., 49, 896 (1973).

[21]K. Kinoshita and H. Noda, Prog. Theor. Phys., 50, 915 (1973).

[22]B. Cox and C. T. Murphy, Nucl. Instr. and Meth., 136, 35 (1976).

[23]R. M. Baltrusaitis et al., Atomic Number Dependence of the Inclusive π^0 Cross Sections at Large $X_\perp$ and X_F, Fermilab-Pub., 79/39-Exp., to be published.

[24]U. Völkel, DESY 67/16 (May, 1967).

[25]B. Cox et al., Fermilab TM-765, 6038.00.

[26]R. M. Baltrusaitis et al., Position Determination of High Energy Photons in Lead Glass, submitted to the 1979 Nuclear Sciences Symposium, (IEEE).

[27]M. S. Goodman et al., Bull. of Am. Phys. Soc., B15, 455 (1973).

TABLE CAPTIONS

Table I: Invariant cross sections $E\frac{d\sigma}{dp^3}$ (cm^2/GeV^2/nucleon) vs. $P_\perp$ for various X_F bands for the reaction pBe $\rightarrow \pi^o$ + X. Linear A dependence has been assumed in calculating the per nucleon cross sections.

Table II: Summary of the two dimensional fits of $E\frac{d\sigma}{dp^3}$ (cm^2/GeV^2/nucleon) to the form $A(1-X_R)^M P_\perp^{-N}$ at 200, 300, and 400 GeV/c.

TABLE I

x_F Region	$P_\perp$ (GeV/c)	$(E\frac{d\sigma}{dp^3})$ 200 GeV	$(E\frac{d\sigma}{dp^3})$ 300 GeV	$(E\frac{d\sigma}{dp^3})$ 400 GeV
0. -.14	1.50-1.75	$(1.20\pm .10)\times10^{-29}$	$(1.57\pm .10)\times10^{-29}$	$(1.03\pm .11)\times10^{-29}$
	1.75-2.00	$(3.83\pm .27)\times10^{-30}$	$(4.76\pm .15)\times10^{-30}$	$(3.80\pm .21)\times10^{-30}$
	2.00-2.25	$(1.17\pm .07)\times10^{-30}$	$(1.51\pm .10)\times10^{-30}$	$(1.47\pm .09)\times10^{-30}$
	2.25-2.50	$(3.81\pm .14)\times10^{-31}$	$(5.23\pm .30)\times10^{-31}$	$(5.49\pm .41)\times10^{-31}$
	2.50-2.75	$(1.31\pm .05)\times10^{-31}$	$(2.06\pm .06)\times10^{-31}$	$(2.22\pm .10)\times10^{-31}$
	2.75-3.00	$(5.31\pm .31)\times10^{-32}$	$(8.76\pm .47)\times10^{-32}$	$(9.41\pm .61)\times10^{-32}$
	3.00-3.25	$(1.76\pm .13)\times10^{-32}$	$(3.53\pm .23)\times10^{-32}$	$(4.77\pm .31)\times10^{-32}$
	3.25-3.50	$(7.60\pm .70)\times10^{-33}$	$(1.36\pm .14)\times10^{-32}$	$(2.07\pm .26)\times10^{-32}$
	3.50-3.75	$(2.82\pm .42)\times10^{-33}$	$(5.83\pm1.11)\times10^{-33}$	$(7.14\pm2.90)\times10^{-33}$
	3.75-4.00	$(7.89\pm3.17)\times10^{-34}$	$(1.71\pm .63)\times10^{-33}$	$(4.63\pm1.41)\times10^{-33}$
	4.00-4.25	$(6.82\pm2.54)\times10^{-34}$	$(1.59\pm .61)\times10^{-33}$	$(1.08\pm .71)\times10^{-33}$
	4.25-4.50	$(4.81\pm2.62)\times10^{-34}$	$(1.33\pm .67)\times10^{-33}$	$(4.04\pm1.48)\times10^{-33}$
-.14--.30	1.75-2.00	-	$(3.06\pm .41)\times10^{-30}$	$(2.69\pm1.20)\times10^{-30}$
	2.00-2.25	$(6.61\pm2.60)\times10^{-31}$	$(8.82\pm .42)\times10^{-31}$	$(9.60\pm1.09)\times10^{-31}$
	2.25-2.50	$(2.47\pm .30)\times10^{-31}$	$(3.29\pm .18)\times10^{-31}$	$(3.14\pm .20)\times10^{-31}$
	2.50-2.75	$(9.97\pm .57)\times10^{-32}$	$(1.25\pm .16)\times10^{-31}$	$(1.25\pm .29)\times10^{-31}$
	2.75-3.00	$(3.62\pm .20)\times10^{-32}$	$(5.14\pm .45)\times10^{-32}$	$(4.84\pm .34)\times10^{-32}$
	3.00-3.25	$(1.35\pm .10)\times10^{-32}$	$(2.04\pm .08)\times10^{-32}$	$(2.38\pm .36)\times10^{-32}$
	3.25-3.50	$(6.60\pm .71)\times10^{-33}$	$(7.77\pm .49)\times10^{-33}$	$(9.69\pm1.05)\times10^{-33}$
	3.50-3.75	$(2.48\pm .22)\times10^{-33}$	$(3.73\pm .34)\times10^{-33}$	$(4.59\pm .42)\times10^{-33}$
	3.75-4.00	$(1.15\pm .13)\times10^{-33}$	$(1.98\pm .23)\times10^{-33}$	$(2.18\pm .20)\times10^{-33}$
	4.00-4.25	$(4.45\pm .75)\times10^{-34}$	$(8.76\pm1.62)\times10^{-34}$	$(1.28\pm .25)\times10^{-33}$
	4.25-4.50	$(2.47\pm .37)\times10^{-34}$	$(4.75\pm .62)\times10^{-34}$	$(4.36\pm .82)\times10^{-34}$
	4.50-4.75	$(7.41\pm1.99)\times10^{-35}$	$(2.55\pm .63)\times10^{-34}$	$(1.29\pm .43)\times10^{-34}$
	4.75-5.00	$(6.05\pm2.18)\times10^{-35}$	$(1.47\pm .75)\times10^{-34}$	$(6.72\pm3.61)\times10^{-35}$
	5.00-5.25	$(2.08\pm1.13)\times10^{-35}$	$(2.11\pm2.17)\times10^{-34}$	$(7.66\pm3.93)\times10^{-35}$
-.30--.50	2.50-2.75	-	$(3.57\pm .83)\times10^{-32}$	-
	2.75-3.00	$(9.69\pm2.30)\times10^{-33}$	$(1.72\pm .12)\times10^{-32}$	-
	3.00-3.25	$(5.15\pm .58)\times10^{-33}$	$(7.51\pm .41)\times10^{-33}$	$(1.96\pm .50)\times10^{-32}$
	3.25-3.50	$(1.81\pm .84)\times10^{-33}$	$(3.42\pm .11)\times10^{-33}$	$(3.56\pm .60)\times10^{-33}$
	3.50-3.75	$(7.93\pm .40)\times10^{-34}$	$(1.51\pm .06)\times10^{-33}$	$(1.88\pm .31)\times10^{-33}$
	3.75-4.00	$(3.62\pm .26)\times10^{-34}$	$(7.50\pm1.06)\times10^{-34}$	$(5.23\pm1.61)\times10^{-34}$
	4.00-4.25	$(1.59\pm .19)\times10^{-34}$	$(2.72\pm .31)\times10^{-34}$	$(5.19\pm1.90)\times10^{-34}$
	4.25-4.50	$(7.24\pm1.30)\times10^{-35}$	$(1.43\pm .18)\times10^{-34}$	$(1.94\pm1.13)\times10^{-34}$
	4.50-4.75	$(2.68\pm .81)\times10^{-35}$	$(9.15\pm1.57)\times10^{-35}$	$(1.40\pm .99)\times10^{-34}$
	4.75-5.00	$(2.31\pm .88)\times10^{-35}$	$(4.56\pm1.13)\times10^{-35}$	-
	5.00-5.25	$(1.01\pm1.01)\times10^{-35}$	$(3.32\pm1.20)\times10^{-35}$	-
	5.25-5.50	-	$(5.67\pm5.68)\times10^{-36}$	-
-.50--.80	3.50-3.75	-	$(1.62\pm .85)\times10^{-34}$	-
	3.75-4.00	$(9.87\pm5.85)\times10^{-35}$	$(5.99\pm1.53)\times10^{-35}$	-
	4.00-4.25	$(9.60\pm6.34)\times10^{-36}$	$(2.44\pm .43)\times10^{-35}$	-
	4.25-4.50	-	$(1.53\pm .29)\times10^{-35}$	-
	4.50-4.75	$(4.59\pm4.59)\times10^{-36}$	$(7.74\pm5.06)\times10^{-36}$	-
	4.75-5.00	$(2.92\pm2.93)\times10^{-36}$	$(4.20\pm1.56)\times10^{-36}$	-
	5.00-5.25	-	$(1.13\pm1.14)\times10^{-36}$	-
	5.25-5.50	$(9.20\pm9.24)\times10^{-37}$	$(3.21\pm2.34)\times10^{-36}$	-
	5.50-5.75	$(5.88\pm5.98)\times10^{-37}$	-	-

TABLE II

Energy (GeV)	X_R	$P_\perp$ (GeV/c)	A	M	N	χ^2/DOF
200	$.1 < X_R < .7$	$1.5 < P_\perp < 5.0$	$3.12 \pm .22 \times 10^{-27}$	$4.81 \pm .16$	$8.90 \pm .12$	1.30
300	$.1 < X_R < .8$	$1.5 < P_\perp < 5.5$	$3.80 \pm .21 \times 10^{-27}$	$4.91 \pm .11$	$8.93 \pm .08$	1.39
400	$.15 < X_R < .5$	$1.5 < P_\perp < 5.5$	$2.91 \pm .22 \times 10^{-27}$	$4.94 \pm .45$	$8.79 \pm .17$	1.63

FIGURE CAPTIONS

Fig. 1: Schematic view of the double arm spectrometer.

Fig. 2a: Two photon mass spectrum 8^{o}-300 GeV/c data - low threshold. (b) Two photon mass spectrum 5.8^{o}-300 GeV/c data-high threshold.

Fig. 3a: Invariant cross section $E\frac{d\sigma}{dp}$, per nucleon vs. $P_{\perp}$ in bands of X_F for pBe collisions at 200 GeV. Linear A dependence is assumed. (b) 300 GeV cross section (c) 400 GeV cross section.

Fig. 4: $P_{\perp}^{9} \cdot E\frac{d\sigma}{dp}$, vs. θ_{cms} at 200 GeV/c for various regions of X_{radial}.

Fig. 5a: $(1-X_R)^{-5} \cdot E\frac{d\sigma}{dp}$, vs. $P_{\perp}$ for 200, 300 and 400 GeV/c data. Independent fits to each data set are shown.

Fig. 5b: $P_{\perp}^{9} \cdot E\frac{d\sigma}{dp}$, vs. X_R for 200, 300, and 400 GeV/c data. Independent fits to each data set are shown.

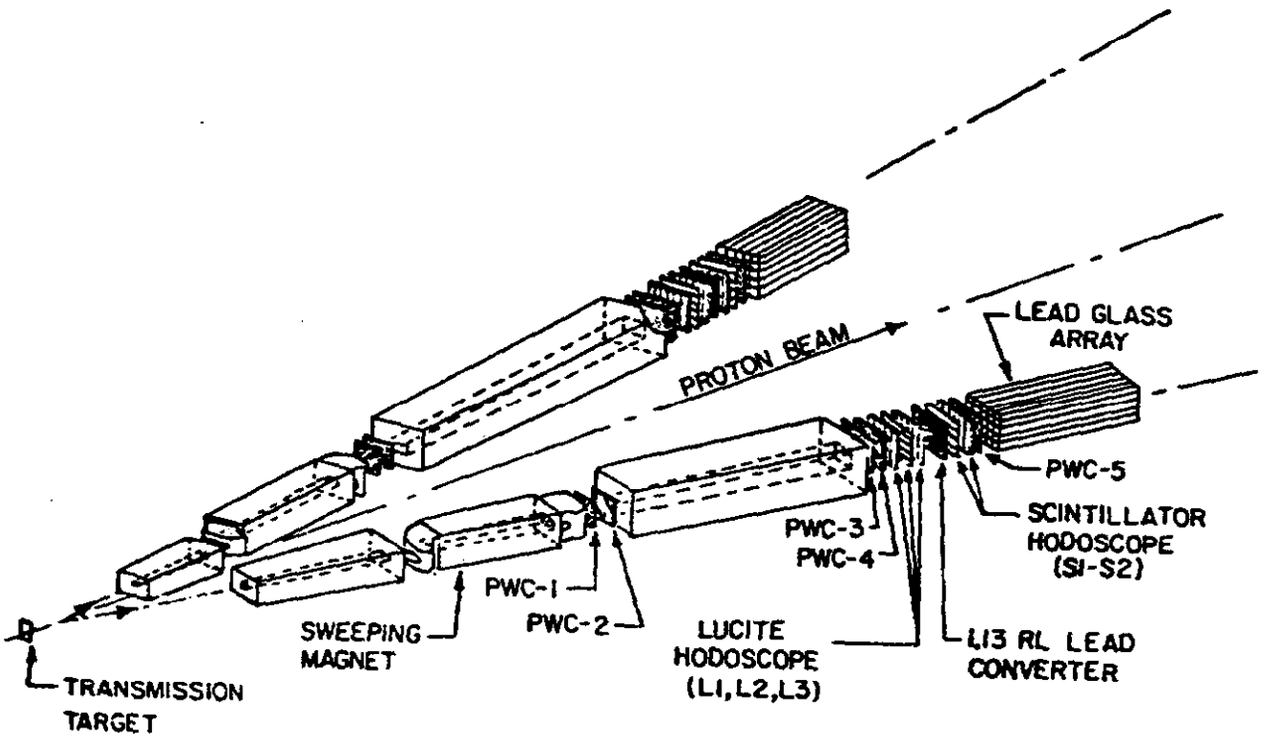
LEAD GLASS
ARRAY
PROTON BEAM
PWC-5
SCINTILLATOR
HODOSCOPE
(S1-S2)
PWC-3
PWC-4
PWC-1
PWC-2
SWEEPING
MAGNET
LUCITE
HODOSCOPE
(L1,L2,L3)
L13 RL LEAD
CONVERTER
TRANSMISSION
TARGET

Fig. 1

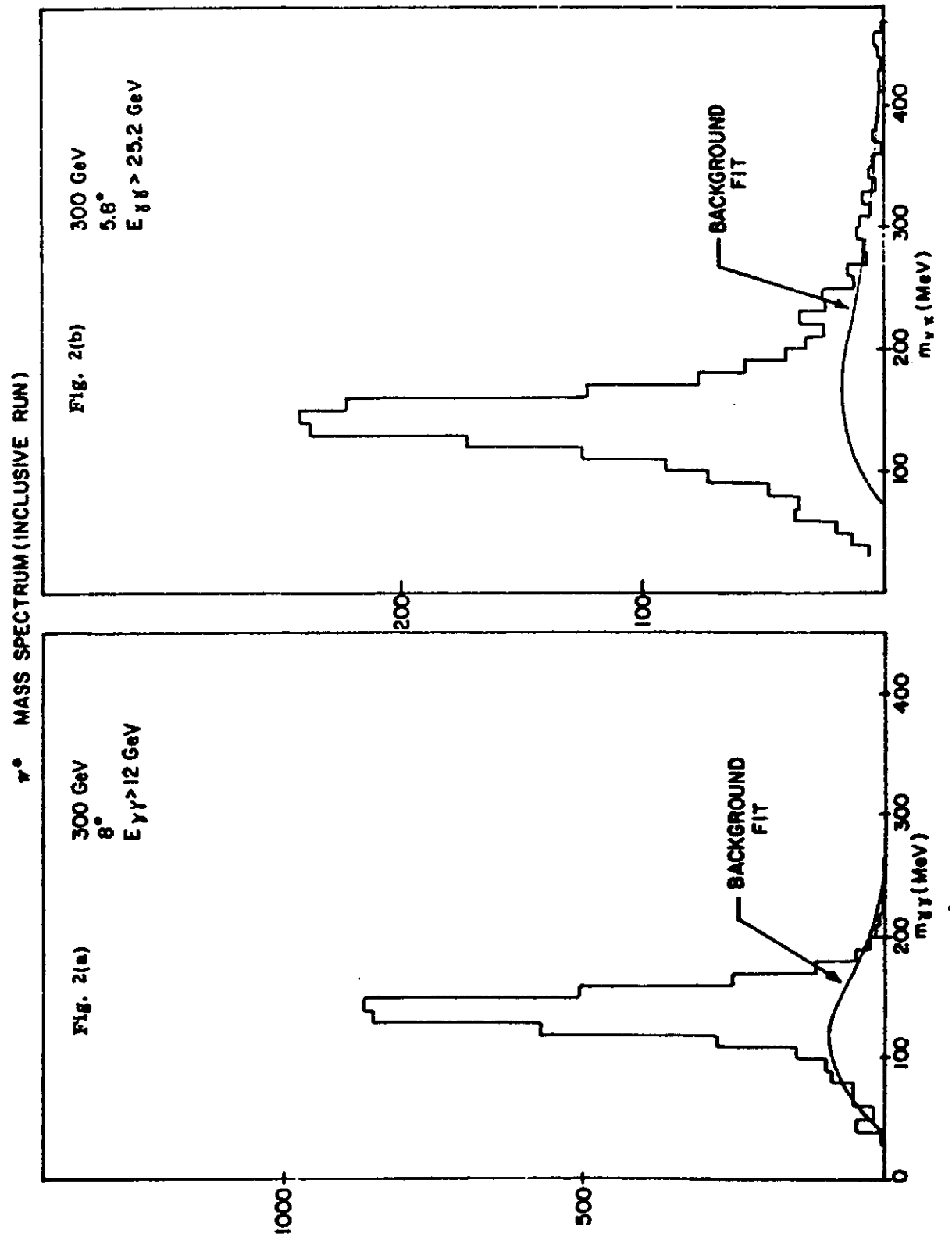
π° MASS SPECTRUM (INCLUSIVE RUN)
Fig. 2(a)
300 GeV
8°
Eγγ>12 GeV
BACKGROUND FIT
Fig. 2(b)
300 GeV
5.8°
Eγγ > 25.2 GeV
BACKGROUND FIT
mγγ (MeV)
0
100
200
300
400
500
1000
100
200

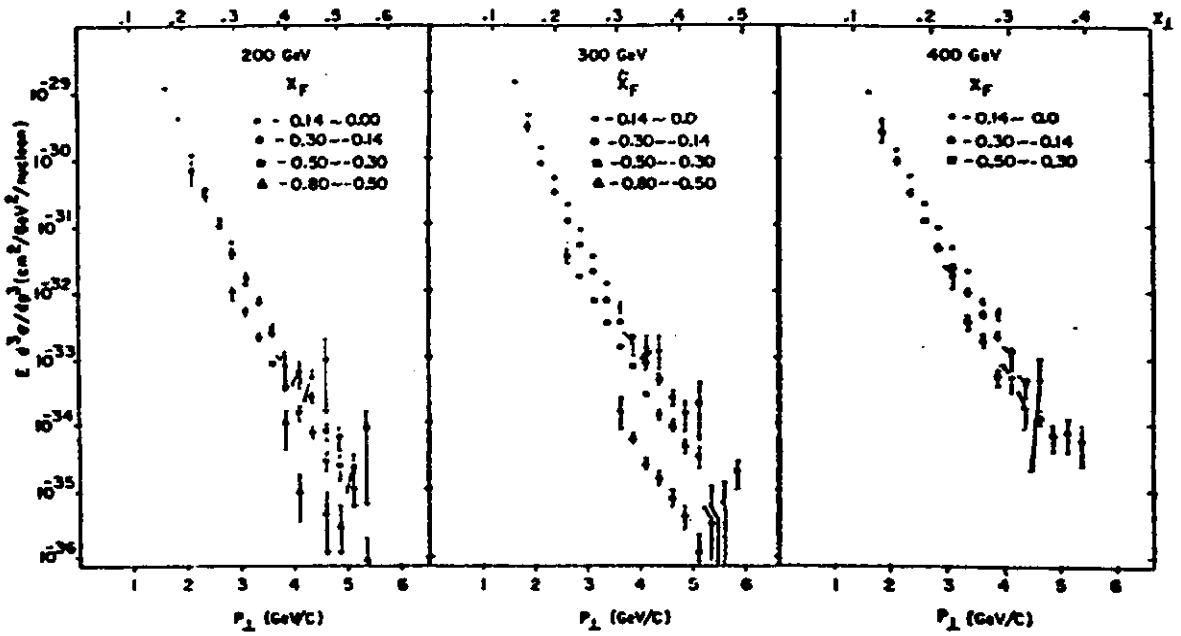

Fig. 3(a) Fig. 3(b) Fig. 3(c)

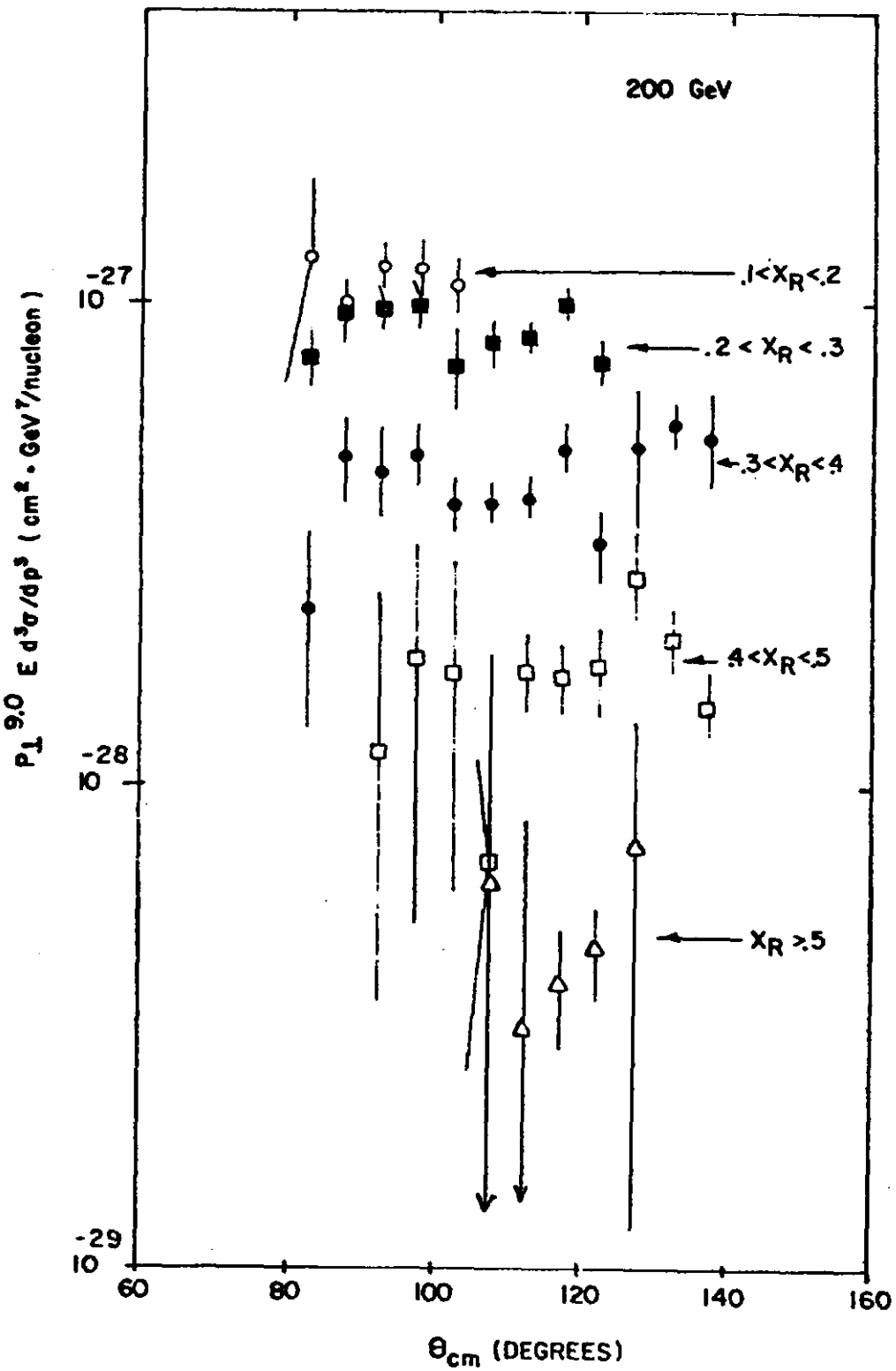
200 GeV
.1<X_R<.2
.2 < X_R < .3
.3<X_R<.4
.4<X_R<.5
X_R >.5
10^-27
10^-28
10^-29
P_T^9.0 E d^3σ/dp^3 (cm^2 · GeV^7/nucleon)
60
80
100
120
140
160
θ_cm (DEGREES)

Fig. 4

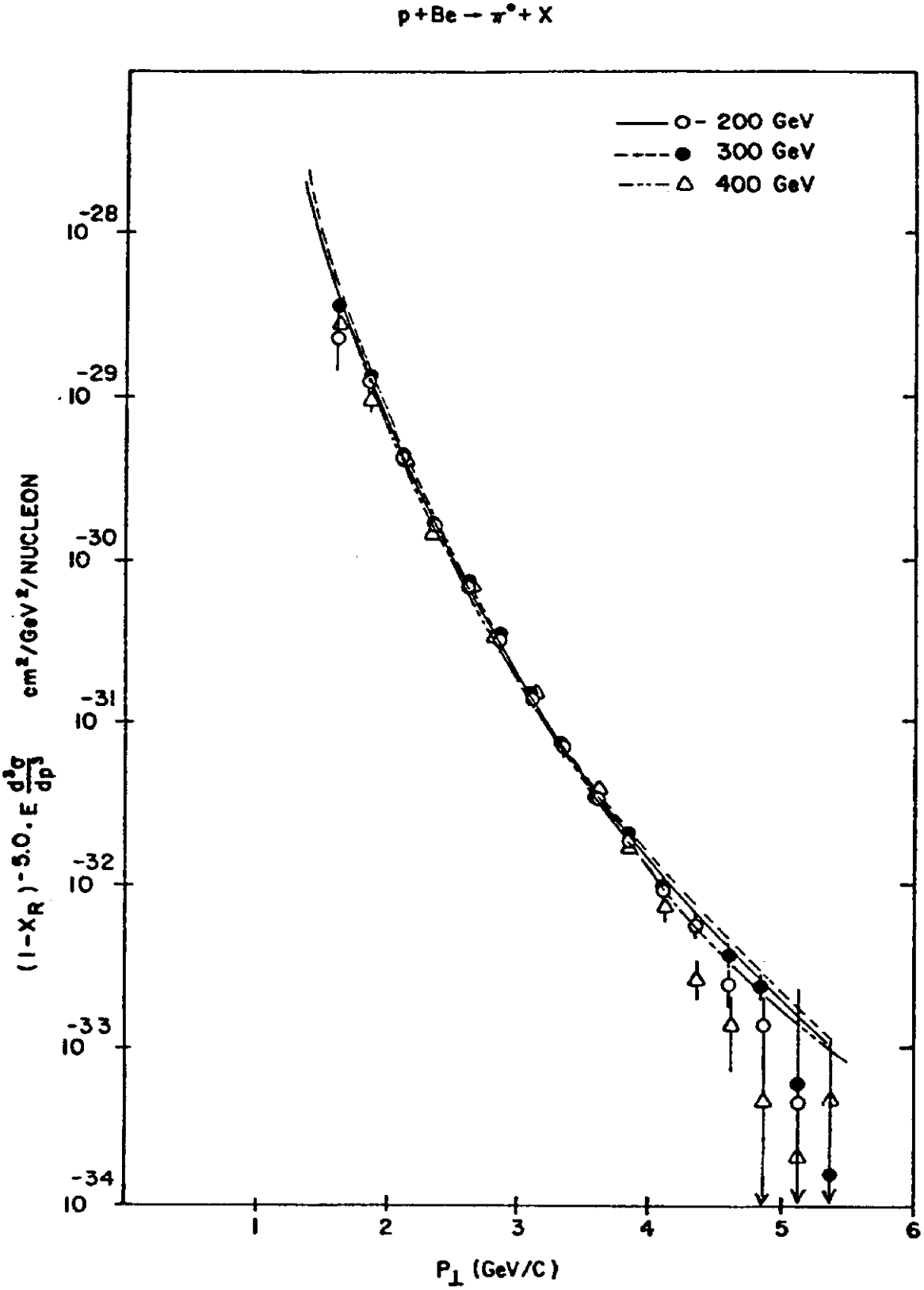
p + Be → π° + X
200 GeV
300 GeV
400 GeV
$(1-X_R)^{5.0} \cdot E \frac{d^3\sigma}{dp^3}$ cm²/GeV²/NUCLEON
10^{-28}
10^{-29}
10^{-30}
10^{-31}
10^{-32}
10^{-33}
10^{-34}
1
2
3
4
5
6
$P_\perp$ (GeV/C)

Fig. 5(a)

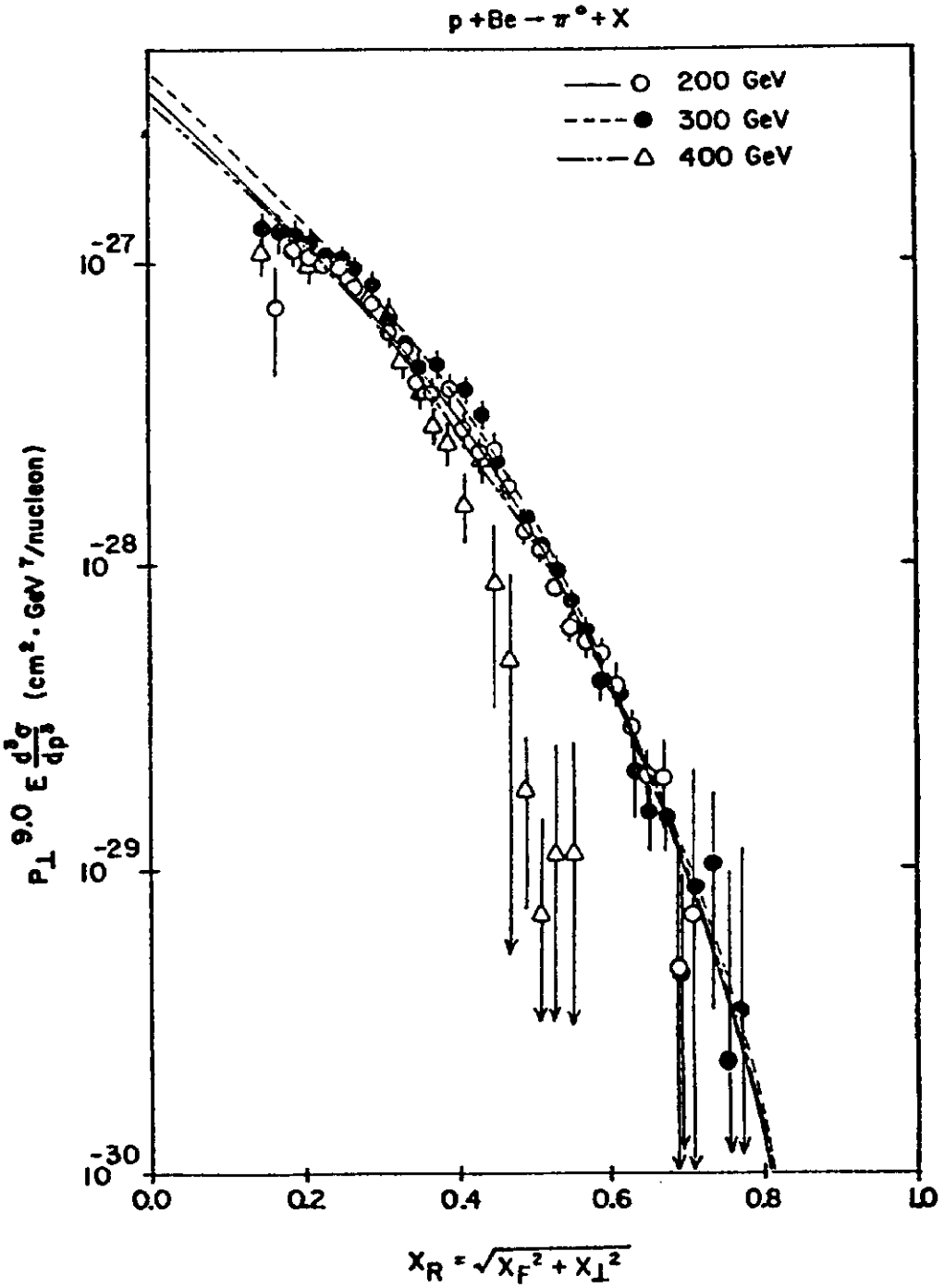
p + Be → π° + X
200 GeV
300 GeV
400 GeV
$P_\perp^{9.0} E \frac{d^3\sigma}{dp^3}$ (cm² · GeV⁷/nucleon)
10^{-27}
10^{-28}
10^{-29}
10^{-30}
0.0
0.2
0.4
0.6
0.8
1.0
$X_R = \sqrt{X_F^2 + X_\perp^2}$

Fig. 5(b)